

Merger-driven infall of metal-poor gas in luminous infrared galaxies: a deep dive beneath the mass-metallicity relation

Borja Pérez-Díaz¹, Enrique Pérez-Montero¹, Juan A. Fernández-Ontiveros², José M. Vílchez¹, Ricardo Amorín^{3,4}

¹*Instituto de Astrofísica de Andalucía (IAA-CSIC), Glorieta de la Astronomía s/n, 18008 Granada, Spain*

²*Centro de Estudios de Física del Cosmos de Aragón (CEFCA), Unidad Asociada al CSIC, Plaza San Juan 1, E-44001 Teruel, Spain*

³*Instituto de Investigación Multidisciplinar en Ciencia y Tecnología, Universidad de La Serena, Raul Bitrán 1305, La Serena, Chile*

⁴*Departamento de Astronomía, Universidad de La Serena, Av. Juan Cisternas 1200 Norte, La Serena, Chile*

The build up of heavy elements and the stellar mass assembly are fundamental processes in the formation and evolution of galaxies. Although they have been extensively studied through observations and simulations, the key elements that govern these processes, such as gas accretion and outflows, are not fully understood¹. This is especially true for luminous and massive galaxies, which usually suffer strong feedback in the form of massive outflows²⁻⁵, and large-scale gas accretion triggered by galaxy interactions⁶⁻⁸. For a sample of 77 luminous infrared (IR) galaxies, we derive chemical abundances using new diagnostics based on nebular IR lines, which peer through the dusty medium of these objects and allow us to include the obscured metals in our abundance determinations. In contrast to optical-based studies, our analysis reveals that most luminous IR galaxies remain close to the mass-metallicity relation. Nevertheless, four galaxies with extreme star-formation rates ($> 60M_{\odot}\text{yr}^{-1}$) in their late merger stages show heavily depressed metallicities of $12+\log(\text{O}/\text{H}) \sim 7.7-8.1$ along with solar-like N/O ratios, indicative of gas mixing processes affecting their chemical composition. This evidence suggests the action of a massive infall of metal-poor gas in a short phase during the late merger stages, eventually followed by a rapid enrichment. These results challenge the classical gas equilibrium scenario usually applied to main-sequence galaxies, suggesting that the chemical enrichment and stellar-mass growth in luminous IR galaxies are regulated by different processes.

The chemical composition of the gas-phase interstellar medium (ISM) is a witness of the evolution of galaxies, as heavy elements (or metals) are produced in stars by stellar nucleosynthesis and eventually ejected into the ISM at the end of their lives⁹. As stellar mass assembly also traces the evolution and formation of galaxies, a natural connection between them arises, materialized in the so-called Mass-Metallicity Relation (MZR)¹⁰⁻¹³ as well as in the Fundamental Metallicity Relation (FZR)^{14,15}, which are regulated by a wide variety

of processes: galaxy environment¹⁶, secular evolution¹⁷, feedback from star-formation¹⁸ and Active Galactic Nuclei (AGN)¹⁹, and stellar age²⁰.

These scaling relations are explained by means of self-regulated equilibrium between gas accretion and star formation¹. However, half of the stellar mass in galaxies that we observe nowadays was formed in a relatively short period of time (~ 3.5 Gyr) during the cosmic noon²¹, i.e., in an extreme scenario where these equilibrium conditions may not apply. Luminous and Ultra-Luminous Infrared Galaxies (LIRGs and ULIRGs, respectively) are key to understanding the complex picture of galaxy evolution, since they allow us to explore nearby galaxies with extreme star formation rates, similar to those found at the cosmic noon²². LIRGs have infrared luminosities $L_{\text{IR}} > 10^{11}L_{\odot}$ by definition, dominate the star-formation activity at $z \sim 1$ and contribute significantly to the cosmic infrared background²³. In addition, ULIRGs with $L_{\text{IR}} > 10^{12}L_{\odot}$ are commonly found in merger systems at $z \gtrsim 2$ and may represent an evolutionary stage in the formation of AGN-hosting galaxies^{24,25}. While the scaling relation between the bulge and central supermassive black holes (SMBHs) in quiescent galaxies suggest a link between accretion rates onto SMBH and the intensity of the episodes of nuclear star formation,^{26,27} the study of (U)LIRGs and their extreme conditions are critical to shed light on the co-evolution of SMBHs and their host galaxies.

Despite the increasing number of studies on the gas-phase ISM metal content in galaxies, the chemical characterization of ULIRGs lacks consensus. On the observational side, optical estimations of the oxygen abundance^{28,29} favour a low-metal content gas scenario for these galaxies. However, this approach presents serious challenges: 1) optical emission lines are significantly affected by dust attenuation, which is particularly important in (U)LIRGs³⁰, and therefore miss the heavy elements located in dust-embedded regions within galaxies; 2) due to the hard ionising radiation field associated with strong starbursts, the cooling process of many metals (such as sulfur, neon or oxygen) may be dominated by highly-ionized species (S^{3+} , Ne^{2+} , and even O^{3+} in some extreme scenarios), whose emission lines are detected in the IR range; and, 3) due to the temperature dependence of optical emission lines, cold regions might remain unobserved. To avoid these problems, studies of the metallicity of ULIRGs from IR emission lines are needed, but such studies are rather scarce and show discrepancies. A study of local ULIRGs using far-IR emission lines was performed on a sample of 20 local galaxies³¹, concluding that $12+\log(O/H)$ ranges from 8.5 to 8.9 [$0.65Z_{\odot}$, $1.65Z_{\odot}$], with many of them found 0.3 dex lower than expected by their position in the MZR. More recently, another study of 5 ULIRGs using again far-IR emission lines showed that, contrary to the previous study, these ULIRGs followed the MZR³² derived for SFGs¹² in the Sloan Digital Sky Survey (SDSS). However, as these studies were performed using ratios of far-IR emission lines (including $[OIII]\lambda 52\mu\text{m}$, $[NIII]\lambda 57\mu\text{m}$, $[OIII]\lambda 88\mu\text{m}$) that are better tracers of the nitrogen-to-oxygen abundance ratio $\log(N/O)$ ^{33,34}, the estimation of $12+\log(O/H)$ relies on the local calibration of the O/H–N/O relation^{39,40}, that might not apply to the case of (U)LIRGs since independent estimations of both quantities lead to subsolar abundances³⁴. On the theoretical side, due to the high dust content³⁵ of ULIRGs, chemical evolution models

predict high metal content in the ISM of these galaxies³⁶. On the other hand, simulations of ULIRGs, as interacting systems, have shown that the chemical content in the gas-phase ISM, mainly traced by the oxygen abundance ($12+\log(\text{O}/\text{H})$), experiences a drop during the merger process^{37,38}. Overall, the lack of a systematic and consistent study of the chemical content in the gas-phase ISM of ULIRGs does not help in solving this problem since an independent determination of the O/H and N/O abundances based on IR emission lines is required to peer through the dusty medium of these galaxies.

In this study, we determine the chemical abundances of the ISM in a sample of 77 (U)LIRGs dominated by star-formation activity, and we use a sample of 55 HII extragalactic regions and star-forming dwarf galaxies as a control sample. Thus, a total sample of 132 galaxies with IR observations is analysed. We use spectroscopic observations of nebular emission lines in the near-, mid- and far-IR ranges acquired with *Spitzer*/IRS, *Herschel*/PACS, and *Akari* for measurements of the Br α emission. To estimate $12+\log(\text{O}/\text{H})$, $\log(\text{N}/\text{O})$ and the ionization parameter $\log(U)$ we use HII-CHI-MISTRY-IR^{34,41}, a code that employs a bayesian-like comparison between the results predicted by large grids of photoionization models with specific observed emission-line ratios. This code allows us to independently estimate these three quantities without assuming any underlying relation between any of them. However if the set of emission lines used as input is reduced (e.g. when no previous estimation of N/O can be provided), the code assumes certain relations that can be changed by the user to find an estimation of the chemical content. For our sample, we use IR emission lines from HII $\lambda 4\mu\text{m}$ to [OIII] $\lambda 88\mu\text{m}$ as input for the code (see Methods for more details). Overall, we find that most galaxies in our sample have a nearly solar metallicity $12+\log(\text{O}/\text{H})\sim 8.6$ ($0.85Z_{\odot}$), which is consistent with previous studies from IR³¹ emission lines. We find a median N/O value for our sample of ~ -1.0 , that is consistent with the expected values for their stellar masses (see Figure 1).

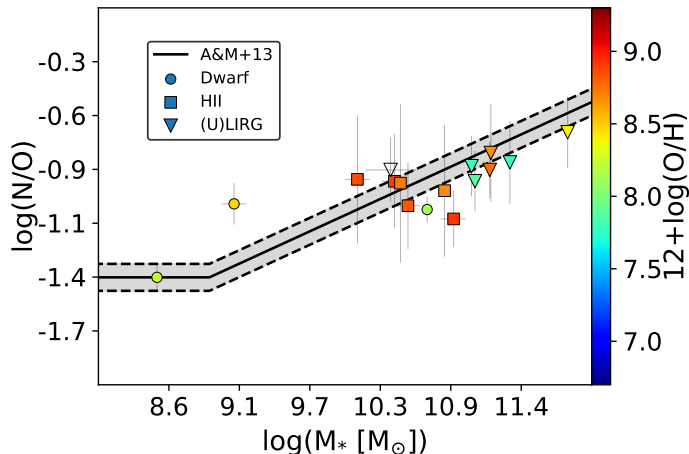


Figure 1 – Relation between stellar mass and nitrogen-to-oxygen ratio for our sample of galaxies. The local relation found for SFGs¹⁰ is shown.

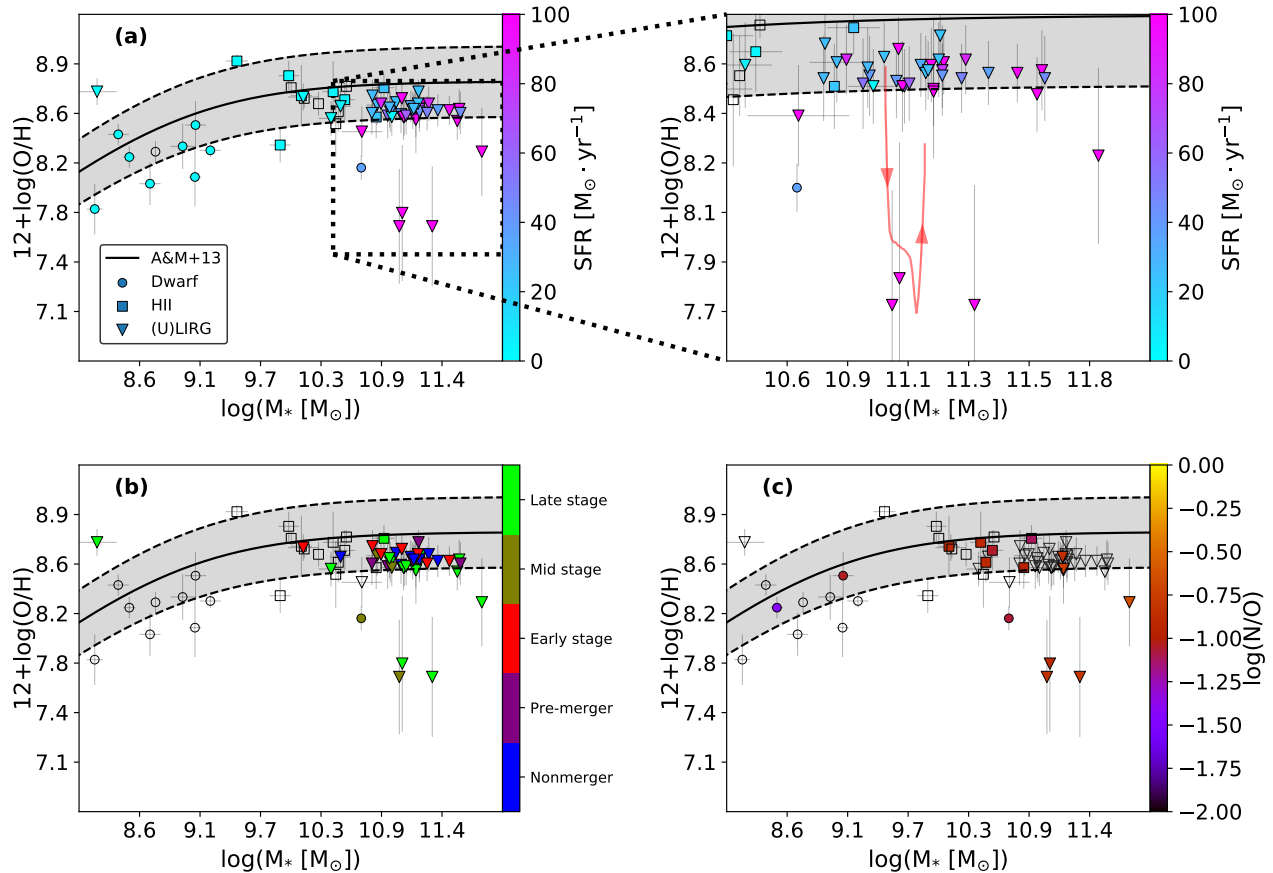


Figure 2 – Mass-metallicity relation for our sample of SFGs. The colorbar shows different properties for their host galaxies: *a*), the star-formation rate (SFR) as retrieved from the literature; *b*), the merger stage as estimated from IRAC $3.6\mu\text{m}$ images; *c*) the N/O chemical ratio. For all plots, blank points are associated with galaxies with no estimations of the colored properties. For plot *a*) we show on the right a zoom with tracks (red line) of an inflow model within the standard evolution of a galaxy⁴² (see Methods for more details on this model).

We present in Figure 2 the MZR for 77 galaxies, including 41 (U)LIRGs, using the oxygen abundances estimated in this work. We compare our results with the MZR previously reported for SFGs¹⁰ (A&M13 track). We find that the large majority of our sample follows the same trend as the rest of SFGs. However, the most massive ULIRGs ($\log(M_*[M_\odot]) > 10.5$) tend to lie towards the low side of the MZR, indicating that they have slightly lower metallicity as compared to the expected value for their stellar mass, confirming what has been also reported in previous studies³¹, although the deviations that we find are smaller than the values found by other studies²⁹. Interestingly, four galaxies namely Haro11, IRAS12112+0305, IRAS20551-4250 and IRAS23128-5919 strongly deviate from the MZR showing metallicities lower by a factor of $\gtrsim 2$ than expected for these *deep-diving* (U)LIRGs stellar masses according

to the MZR. While Haro11 is not a ULIRG galaxy like the others, this star-forming galaxy is reported to be a well known merger dominated galaxy that shared many of properties^{43,44} observed in ULIRGs. Notably, IRAS12112+0305 was previously reported to have a super-solar abundance ($\sim 2Z_{\odot}$)³², while IRAS20551-4250 and IRAS23128-5919 were reported to have abundances close to the values expected from the MZR at their masses⁴⁵. These high estimations of O/H are driven by the nearly solar N/O values obtained here. However, our O/H estimation – independent of N/O – is significantly lower, thus suggesting a more complex mixing process of the gas affecting their chemical composition. These deviations from the local relation between N/O–O/H found in SFGs have been also reported for other types of galaxies such as *Green Pea* Galaxies⁴⁶.

We show in Figure 2 that these *deep-diving* (U)LIRGs have the highest SFR values in our sample ($> 100 M_{\odot}\text{yr}^{-1}$) and they are in the final stages of their mergers. Additionally, we find that the N/O ratios for these four galaxies are similar to the solar ratio, which suggests that they have reached a relatively mature stage of their chemical enrichment history^{46,47}. These results imply that during the merging process of (U)LIRGs, metal-poor gas is accreted towards the central region of the galaxies, which dilutes the metal abundances relative to hydrogen, fuels star formation, but keeps the N/O ratio unaffected because it is independent of the effects of a massive infall of hydrogen. Additionally, intermediate-massive stars of these galaxies do not have enough time to boost the nitrogen production from CNO cycles⁴⁸. As also shown in Figure 3 a), these *deep-diving* (U)LIRGs also deviate from the FZR relation, implying that these (U)LIRGs are mainly out of the self-regulated equilibrium between gas accretion and star formation.

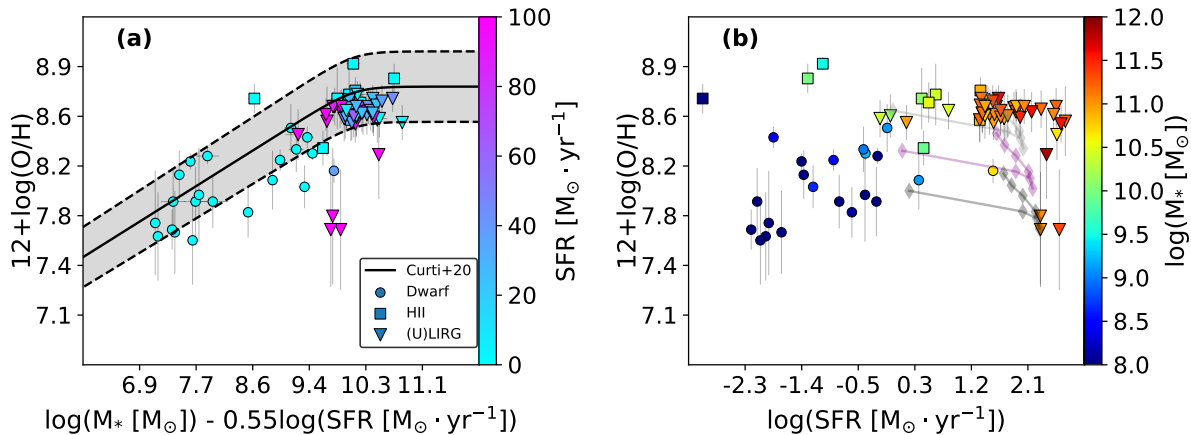


Figure 3 – Relations between SFR, stellar mass and metallicity. *a)* shows the FMR relation for $\log(M_* [M_{\odot}]) - \alpha \log(\text{SFR} [M_{\odot}\cdot\text{yr}^{-1}])$ assuming $\alpha = 0.55$ ¹⁵. *b)* shows the relation between O/H and SFR for our sample of galaxies, while semi-transparent lines represent tracks obtained in simulations of mergers of galaxies with the same stellar mass³⁷, considering different initial conditions.

To strengthen the case for massive infall of gas in these *deep-diving* (U)LIRGs, we discuss two models of inflow that reproduce the trends of these inflows. In Figure 2 *a*), we present a basic inflow model⁴², in which the analyzed galaxy (or common envelope of two galaxies) experiences a drop of metallicity over a period of time between 100 to 1000 Myr. These timescales further support our scenario and explain why only four galaxies (*deep-diving* (U)LIRGs) in our sample were captured in the process, as these timescales are really short for a ~ 12 Gyr old-like galaxy. Once the merger process is completed and stars begin to pollute the ISM again, the resulting galaxy increases its metallicity. According to this model, an additional contribution from outflows is necessary for the merger to recover the metallicity expected from the MZR for a galaxy of that stellar mass. This is in line with the metal-loaded outflows often found in ULIRGs²⁻⁵. In Figure 3 *b*) we present tracks that correspond to different stages in a merger process between two galaxies of similar masses, as inferred from simulations³⁷ in the SFR-O/H relation which is known to play an important role in the MZR^{1,14,15,20}. While these trends are dependent on the initial conditions of the involved galaxies, they all point towards a drop in metallicity which corresponds to a period of time of 600-850 Myr during the merger process³⁷, consistently with the times derived for our inflow model.

In summary, our study reveals that (U)LIRGs exhibit *loops* in the MZR due to the rapid infall of massive clouds of metal-poor gas that promote violent star formation in these galaxies. This scenario explains several observed properties of (U)LIRGs, including the discrepancy among different chemical models in reproducing the dust content of these galaxies, the required fuel to sustain their high star formation rates, and the anomalous low metal content of mid- and late-merger stage galaxies despite their high N/O ratios indicative of an advanced chemical stage. Both simulations and simple inflow models can reproduce this scenario, and once the inflow phase is complete, the role of outflows is crucial for the galaxy to regain its initial metal content. Under these conditions, the build up of heavy elements and the stellar mass growth are not self-regulated by the same gas equilibrium prescription applied to main-sequence galaxies. Overall, due to the short timescales during which the inflow phase can be captured, only a few galaxies in our sample demonstrate clear evidence of this scenario.

References

1. Maiolino, R. & Mannucci, F. De re metallica: the cosmic chemical evolution of galaxies. *A&A Rev.* **27**, 3 (2019).
2. Arribas, S., Colina, L., Bellocchi, E., Maiolino, R. & Villar-Martín, M. Ionized gas outflows and global kinematics of low-z luminous star-forming galaxies. *Astron. Astrophys.* **568**, A14 (2014).
3. Cazzoli, S., Arribas, S., Maiolino, R. & Colina, S. Neutral gas outflows in nearby [U]LIRGs via optical NaD feature. *Astron. Astrophys.* **590**, A125 (2016).
4. Cicone, C., *et al.* Massive molecular outflows and evidence for AGN feedback from CO observations. *Astron. Astrophys.* **590**, A125 (2016).
5. Pereira-Santaella, M., *et al.* Spatially resolved cold molecular outflows in ULIRGs. *Astron. Astrophys.* **616**, A171 (2018).
6. Joseph, R. D. & Wright, G. S. Recent star formation in interacting galaxies - II. Super starbursts in merging galaxies. *Mon. Not. R. Astron. Soc.* **214**, 87-95 (1985).
7. Howell, J. H. *et al.* The Great Observatories All-sky LIRG Survey: Comparison of Ultraviolet and Far-infrared Properties. *Astrophys. J.* **715**, 572-588 (2010).
8. Kennicutt, R. C. & Evans, N. J. Star Formation in the Milky Way and Nearby Galaxies. *ARA&A* **50**, 531-608 (2012).
9. Nomoto, K., Kobayashi, C. & Tominaga, N. Nucleosynthesis in Stars and the Chemical Enrichment of Galaxies. *ARA&A* **51**, 457-509 (2013).
10. Andrews, B. H. & Martini, P. The Mass-Metallicity Relation with the Direct Method on Stacked Spectra of SDSS galaxies. *Astrophys. J.* **765**, A140 (2013).
11. Lequeux, J., Peimbert, M., Rayo, J. F., Serrano, A. & Torres-Peimbert, S. Chemical Composition and Evolution of Irregular and Blue Compact Galaxies. *Astron. Astrophys.* **80**, 155 (1979).
12. Tremonti, C. A. *et al.* The Origin of the Mass-Metallicity Relation: Insights from 53,000 Star-forming Galaxies in the Sloan Digital Sky Survey. *Astrophys. J.* **613**, 898-913 (2004).
13. Pérez-Montero, E. *et al.* The dependence of oxygen and nitrogen abundances on stellar mass from the CALIFA survey. *Astron. Astrophys.* **595**, A62 (2016).
14. Mannucci, F., Cresci, G., Maiolino, R., Marconi, A. & Gnerucci, A. A fundamental relation between mass, star formation rate and metallicity in local and high-redshift galaxies. *Mon. Not. R. Astron. Soc.* **408**, 2115-2127 (2010).

15. Curti, M., Mannucci, F., Cresci, G. & Maiolino, R. The mass-metallicity and the fundamental metallicity relation on a fully T_e -based abundance scale for galaxies. *Mon. Not. R. Astron. Soc.* **491**, 944-964 (2020).
16. Peng, Y. & Maiolino, R. The dependence of the galaxy mass-metallicity relation on environment and the implied metallicity of the IGM. *Mon. Not. R. Astron. Soc.* **438**, 262-270 (2014).
17. Somerville, R. S. & Davé, R. Physical Models of Galaxy Formation in a Cosmological Framework. *ARA&A* **53**, 51-113 (2015).
18. Blanc, G. A., Lu, Y., Benson, A., Katsianis, A. & Barraza, M. A Characteristic Mass Scale in the Mass-Metallicity Relation of Galaxies. *Astrophys. J.* **877**, A6 (2019).
19. Thomas, A. D., Kewley, L. J., Dopita, M. A., Groves, B. A., Hopkins, A. M. & Sutherland, R. S. The Mass-Metallicity Relation of Local Active Galaxies. *Astrophys. J.* **874**, A100 (2019).
20. Duarte-Puertas, S. *et al.* Mass-metallicity and star formation rate in galaxies: A complex relation tuned to stellar age. *Astron. Astrophys.* **666**, A186 (2022).
21. Förster Schreiber, N. M. & Wuyts, S. Star-Forming Galaxies at Cosmic Noon. *ARA&A* **58**, 661–725 (2020).
22. Armus, L. *et al.* GOALS: The Great Observatories All-Sky LIRG Survey. *PASP* **121**, 559 (2009).
23. Stierwalt, S. *et al.* Mid-infrared Properties of Nearby Luminous Infrared Galaxies. I. Spitzer Infrared Spectrograph Spectra for the GOALS Sample. *Astrophys. J. Supp.* **206**, A1 (2013).
24. Sanders, D. B. *et al.* Ultraluminous Infrared Galaxies and the Origin of Quasars. *Astrophys. J.* **325**, 74 (1988).
25. Evans, A. S., Mazzarella, J. M., Surace, J. A., Frayer, D. T., Iwasawa, K. & Sanders, D. B. Molecular Gas and Nuclear Activity in Radio Galaxies Detected by IRAS. *Astrophys. J. Supp.* **159**, 197-213 (2005).
26. Gebhardt, K. *et al.* Black Hole Mass Estimates from Reverberation Mapping and from Spatially Resolved Kinematics. *Astrophys. J.* **543**, L5-L8 (2000).
27. Magnelli, B. *et al.* The $0.4 < z < 1.3$ star formation history of the Universe as viewed in the far-infrared. *Astron. Astrophys.* **496**, 57-75 (2009).
28. Caputi, K. I. *et al.* The Optical Spectra of 24 μm Galaxies in the COSMOS Field. I. Spitzer MIPS Bright Sources in the zCOSMOS-Bright 10k Catalog. *Astrophys. J.* **680**, 939-961 (2008).

29. Rupke, D. S. N., Veilleux, S. & Baker, A. J. The Oxygen Abundances of Luminous and Ultraluminous Infrared Galaxies. *Astrophys. J.* **674**, 172-193 (2008).
30. Franceschini, A. *et al.* An XMM-Newton hard X-ray survey of ultraluminous infrared galaxies. *Mon. Not. R. Astron. Soc.* **343**, 1181-1194 (2003).
31. Pereira-Santaella, M., Rigopoulou, D., Farrah, D., Lebouteiller, V. & Li, J. Far-infrared metallicity diagnostics: application to local ultraluminous infrared galaxies. *Mon. Not. R. Astron. Soc.* **470**, 1218-1232 (2017).
32. Chartab, N. *et al.* Low gas-phase metallicities of ultraluminous infrared galaxies are a result of dust obscuration. *Nat. Astron.* **6**, 844-849 (2022).
33. Peng, J. A. *et al.* Far-Infrared Line Diagnostics: Improving N/O Abundance Estimates for Dusty Galaxies. *Astrophys. J.* **908**, 166 (2021).
34. Fernández-Ontiveros, J. A., Pérez-Montero, E., Vílchez, J. M., Amorín, R. & Spinoglio, L. Measuring chemical abundances with infrared nebular lines: HII-CHI-MISTRY-IR. *Astron. Astrophys.* **652**, A23 (2021).
35. Herrero-Illana, R. *et al.* Molecular gas and dust properties of galaxies from the Great Observatories All-sky LIRG Survey. *Astron. Astrophys.* **628**, A71 (2019).
36. Calura, F & Matteucci, F. Cosmic evolution of metal densities: the enrichment of the intergalactic medium. *Mon. Not. R. Astron. Soc.* **369**, 465-478 (2006).
37. Montuori, M. *et al.* The dilution peak, metallicity evolution, and dating of galaxy interactions and mergers. *Astron. Astrophys.* **518**, A56 (2010).
38. Rupke, D. S. N., Kewley, L. J. & Galaxy Mergers and the Mass-Metallicity Relation: Evidence for Nuclear Metal Dilution and Flattened Gradients from Numerical Simulations. *Astrophys. J.* **710**, L156-L160 (2010).
39. Pérez-Montero, E. & Contini, T. The impact of the nitrogen-to-oxygen ratio on ionized nebula diagnostics based on [NII] emission lines. *Mon. Not. R. Astron. Soc.* **398**, 949-960 (2009).
40. Pérez-Montero, E. Deriving model-based T_e -consistent chemical abundances in ionized gaseous nebulae. *Mon. Not. R. Astron. Soc.* **441**, 2663-2675 (2014).
41. Pérez-Díaz, B., Pérez-Montero, E., Fernández-Ontiveros, J. A. & Vílchez, J. M. Measuring chemical abundances in AGN from infrared nebular lines: HII-CHI-Mistry-IR for AGN. *Astron. Astrophys.* **666**, A115 (2022).
42. Köppen, J. & Edmunds, M. G. Gas flows and the chemical evolution of galaxies - III. Graphical analysis and secondary elements. *Mon. Not. R. Astron. Soc.* **306**, 317-326 (1999).

43. Östlin, G. *et al.* Kinematics of Haro 11: The miniature Antennae. *Astron. Astrophys.* **583**, A55 (2015).
44. Östlin, G. *et al.* The Source of Leaking Ionizing Photons from Haro11: Clues from HST/COS Spectroscopy of Knots A, B and C. *Astrophys. J.* **912**, 155 (2021).
45. Herrera-Camus, R. *et al.* SHINING, A Survey of Far-infrared Lines in Nearby Galaxies. II. Line-deficit Models, AGN Impact, [CII]-SFR scaling relations, and Mass-Metallicity Relation in (U)LIRGs. *Astrophys. J.* **861**, 95 (2018).
46. Amorín, R. O., Pérez-Montero, E. & Vílchez, J. M. On the Oxygen and Nitrogen Chemical Abundances and the Evolution of the "Green Pea" Galaxies. *Astrophys. J.* **715**, L128-L130 (2010).
47. Pérez-Montero, E. *et al.* The cosmic evolution of oxygen and nitrogen abundances in star-forming galaxies over the past 10 Gyr. *Astron. Astrophys.* **549**, A25 (2013).
48. Vincenzo, F. & Kobayashi, C. Evolution of N/O ratios in galaxies from cosmological hydrodynamical simulations. *Mon. Not. R. Astron. Soc.* **478**, 155-166 (2018).

Acknowledgements BPD, EPM and JVM acknowledge financial support from the grant CEX2021-001131-S funded by MCIN/AEI/ 10.13039/501100011033. BPD, EPM and JVM also acknowledge support from the Spanish MINECO grants AYA2016-76682C3-1-P, AYA2016-79724-C4 and PID2019-106027GB-C41. JAFO acknowledges the financial support from the Spanish Ministry of Science and Innovation and the European Union – NextGenerationEU through the Recovery and Resilience Facility project ICTS-MRR-2021-03-CEFCA, and the grant PDG2021-124918-NB-C44. RA acknowledges support from ANID Fondecyt Regular 1202007. EPM acknowledges the assistance from his guide dog Rocko without whose daily help this work would have been much more difficult.

Author Contributions BPD, EPM and JAFO authored the draft version of this paper. BPD and JAFO compiled the sample of galaxies from the literature as well as all the ancillary data required for the analysis. EPM and BPD developed the code used to estimate chemical abundances. JVM and RA supervised the models and contributed to interpreting the results and contributed to the improvement of this manuscript.

Correspondence Correspondence for materials should be addressed to B. P.-D. (bperez@iaa.es), E. P.-M. (epm@iaa.es) and J. A. F.-O. (j.a.fernandez.ontiveros@gmail.com)

Competing interests statement The authors declare no competing interests.

Methods

Here we provide more detailed information in the selection of the sample (§ 1) of Ultra-Luminous Infrared Galaxies (ULIRGs) and Star-forming Galaxies (SFGs) with IR spectroscopic data. We also described the methodology employed to estimate the chemical content of the gas-phase interstellar medium (ISM) in our sample (§ 2). In addition, we give some details about the retrieval of other properties derived in the sample, such as the stellar mass (M_*), the star-formation rate (SFR), or the merger stage (§ 3). Finally, we present in detail some evolutionary models that reproduce the behaviour of our sample of galaxies (§ 4). Throughout this study, we assume as reference system the solar chemical abundances⁴⁶.

1 The sample of Ultra-luminous Infrared Galaxies and Star-forming Galaxies

1.1 Selection

We build our sample of galaxies with IR spectroscopic data from two different catalogs. The first one was retrieved from the IDEOS^{53,54} IR database, which includes the measurements of 77 fitted mid-IR observables in the range 5.4-36 μm for all galaxies observed with *Spitzer* (a total of 3335 galaxies⁵⁴). From this initial sample, we omit duplicate observations of one single object and entries corresponding to galaxies presented in the first catalog, where the higher resolution spectroscopic observation was taken. After verifying that star formation dominates the ionisation budget in our final sample of galaxies (see next subsection), we perform a cross-match with an *AKARI* sample of ULIRGs⁵⁵ to provide measurements of at least one hydrogen recombination line, particularly H I (5-4). In all, a total sample of 66 ULIRGs was retrieved.

The second catalog³⁴ consists of a sample of dwarf galaxies, SFGs, and ULIRGs that present mid- to far-IR range spectroscopic observations from the InfraRed Spectrograph (IRS⁴⁷) on board *Spitzer* and from the Photodetector Array Camera and Spectrometer (PACS⁴⁸) on board *Herschel*^{34,49}. We compiled measurements for a sample of 66 galaxies showing detections of [OIII] $\lambda 52\mu\text{m}$ and [NIII] $\lambda 57\mu\text{m}$ far-IR lines³³ from the IFU spectroscopy instrument FIFI-LS⁵⁰ on board the SOFIA airborne observatory. Additionally, we obtained measurements of hydrogen recombination lines H I (7-6) and (5-4) from the *Spitzer* calibrated spectra available in the CASSIS⁵² database and from observations via AKARI/IRC⁵¹, respectively.

1.2 Classification

For the first sample of galaxies, the ratio between [NeV] $\lambda 14\mu\text{m}$ and [NeII] $\lambda 12\mu\text{m}$ ensures^{31,34} an AGN contamination lower than 10%. For the second sample, we use two criteria^{56,57} both based on the relative emission of high ionic species ([NeV] $\lambda 14\mu\text{m}$ and [OIV] $\lambda 26\mu\text{m}$) to low

ionic species ($[\text{NeII}]\lambda 12\mu\text{m}$) and on the strength of the polycyclic aromatic hydrocarbon (PAH) at $11.25\mu\text{m}$, since AGN activity is expected to enhance higher ionic species^{41,59} and the equivalent width (EW) of PAHs has been proposed⁵⁸ as a tracer of the star-formation activity.

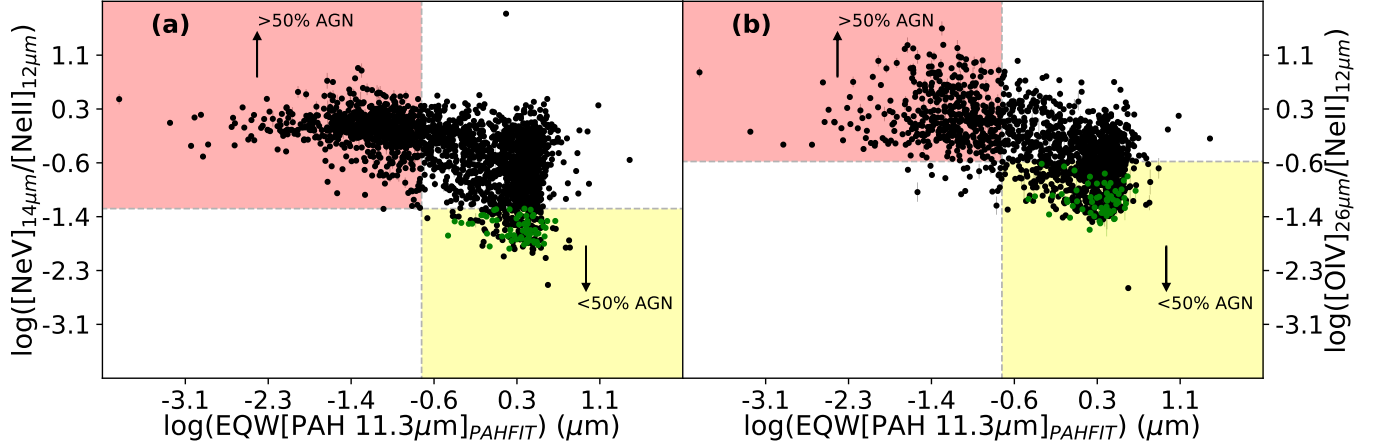


Figure 4 – Diagnostic diagrams for the AGN contamination^{56,57} based on IR spectral features. The whole sample of galaxies from IDEOS is presented in these plots, while the sample of (U)LIRGs retrieved is highlighted in green. *a*) Diagnostic diagram using $[\text{NeV}]\lambda 14\mu\text{m}$ as a high-ionized specie. *b*) Diagnostic diagram using $[\text{OIV}]\lambda 26\mu\text{m}$ instead.

In Figure 4 we present both criteria for the sample of galaxies retrieved from IDEOS. To ensure the robustness in the classification and avoid AGN contamination in first order, we only select galaxies which belong to the SF-dominated region (yellow shaded region) in both diagrams. Moreover, when compared our classification to that presented in IDEOS⁵⁴, we found that the whole selected sample (66 galaxies) show silicate strength and an equivalent width for the PAH at $6.2\mu\text{m}$ also compatible with star-forming dominated activity.

2 Chemical abundance estimations

The estimation of chemical abundances, the oxygen content ($12+\log(\text{O}/\text{H})$) and the nitrogen-to-oxygen ratio ($\log(\text{N}/\text{O})$), as well as the ionization parameter ($\log(\text{U})$) was performed using HII-CHI-MISTRY-IR^{34,41} (or HCM-IR). In brief, HCM-IR[†] is a python code that performs a Bayesian-like calculation of the above mentioned quantities by comparing a set of emission lines with the predictions calculated from a grid of photoionization models⁴⁰. By default, the code provides four different grids of models, varying the Spectral Energy Distribution (SED) used as ionization source. For our study, since our sample is dominated by star-formation, we use the POPSTAR grid, which was computed assuming a SED of

[†]All versions of the HII-CHI-MISTRY code are publicly available at: <http://www.iaa.csic.es/~epm/HII-CHI-mistry.html>.

simple stellar population models from POPSTAR⁶⁰, assuming a constant density of 100 cm^{-3} , a filling factor of 0.1 and plane-parallel geometry. Previous studies of the code have shown that these assumptions do not introduced large uncertainties in the derived abundances, although some differences can be found in the ionization parameter^{40,41,59,61–63}. The grid covers a range in $12+\log(\text{O}/\text{H})$ from 6.9 to 9.1 in bins of 0.1 dex, in $\log(\text{N}/\text{O})$ from -2.0 to 0.0 in bins of 0.125 dex and in $\log(\text{U})$ from -4.0 to 1.5 in bins of 0.25 dex.

The lines accepted by the code in the input include $\text{H}\text{I}\lambda 4.05\mu\text{m}$, $[\text{Ar}\text{II}]\lambda 6.99\mu\text{m}$, $\text{H}\text{I}\lambda 7.46\mu\text{m}$, $[\text{Ar}\text{III}]\lambda 8.99\mu\text{m}$, $\text{H}\text{I}\lambda 12.4\mu\text{m}$, $[\text{Ne}\text{II}]\lambda 12.8\mu\text{m}$, $[\text{Ne}\text{V}]\lambda 14.3\mu\text{m}$, $[\text{Ne}\text{III}]\lambda 15.6\mu\text{m}$, $[\text{Ne}\text{V}]\lambda 24\mu\text{m}$, $[\text{O}\text{IV}]\lambda 26\mu\text{m}$, $[\text{O}\text{III}]\lambda 52\mu\text{m}$, $[\text{N}\text{III}]\lambda 57\mu\text{m}$, $[\text{O}\text{III}]\lambda 88\mu\text{m}$. As compared to previous versions of the code employed for other samples of SFGs³⁴ or AGNs⁴¹, we introduce two modifications (version 3.1). The first modification is that the input now accepts argon emission lines, which behave in the same way as neon emission lines. Secondly, the code does no longer use sulfur emission lines to derive the oxygen abundance ratio as they are used instead to estimate the sulfur content independently from the oxygen estimation. Some authors^{64,65} have pointed that sulfur-to-oxygen ratios might deviate from the solar ratio in the low- and high-metal regime, implying that the use of sulfur emission lines to estimate the oxygen content might introduce a bias. The code finds solutions for $12+\log(\text{O}/\text{H})$, $\log(\text{N}/\text{O})$ and $\log(\text{U})$ as the average of the χ^2 -weighted distribution of all models, being χ^2 the quadratic differences between the observed and the predicted emission-line ratios sensitive to the above chemical ratios built upon the emission lines cited above. The code performs an independent estimation of $\log(\text{N}/\text{O})$ and $12+\log(\text{O}/\text{H})$, although if N/O cannot be constrained due to the lack of key emission lines, a relation between O/H and N/O is assumed by the code. By default, this relation is the one obtained for star-forming regions using chemical abundances based on optical emission-lines^{39,40}. In this work, as N/O can be estimated independently from far-IR emission lines, this relation is not used.

3 Ancillary data

To perform our study, we have retrieved almost all properties that are key in understanding the chemical evolution of the galaxies, i.e., the stellar mass, the star-formation rate or the merger state. In this section, we detail how we obtained these values from the literature and the methodologies followed to estimate them.

3.1 Stellar mass and star formation rates

For 30 galaxies, we retrieved their stellar masses and star formation rates from the Great Observatories All-sky LIRG Survey (GOALS^{7,22}). Particularly, the SFR was estimated from the *IRAS* L_{IR} and from *GALEX* FUV, which provides an estimation of the unobscured and obscured SFR respectively⁷. The stellar mass was estimated from photometry using IRAC $3.6\mu\text{m}$ and Two Micron All Sky Survey (2MASS) K-band photometry.

For 21 galaxies, we retrieve their stellar masses and SFRs from the GALSPEC Data Release 8^{12,66,67}. Particularly, these quantities were retrieved following a Bayesian technique to match two stellar absorption indices, the $D_n(4000)$ break⁶⁸ and the $H\delta_A$ Balmer absorption-line index⁶⁹, from a library of different star formation histories from Monte Carlo realizations⁶⁶.

For ten galaxies, we retrieved their stellar masses⁷⁰ derived from *WISE* bands W1 and W2 following the GAMA-derived stellar mass-to-light ratio relation⁷¹. Their SFRs were obtained from *WISE* bands W1 and W3 to estimate the Balmer-decrement-corrected $H\alpha$ luminosity^{70,72,73}.

For seven galaxies, we retrieved their stellar masses from the S⁴G⁷⁴⁻⁷⁷ sample, which were estimated from the 2MASS photometry⁷⁸. For these seven galaxies, we could not retrieve their SFRs. For another four galaxies, we obtained their stellar masses from the catalog published for a subsample of galaxies from the CASSIS database whose stellar masses and SFRs were obtained after applying the photometric SED fitting code CIGALE^{79,80} to their UV and near-IR observations⁸¹.

3.2 Merger stage

The GOALS sample also offers²³ an estimation of the merger stage based on observations via IRAC 3.6 μ m images. By visual inspection, the authors provide a classification in the following categories: *nonmergers* when there is no sign of merger activity or its neighborhood lacks massive galaxies; *pre-mergers*, if the images reveal a pair of galaxies prior to the first encounter; *early-stage mergers*, pair of galaxies after the first encounter; *mid-stage mergers*, if they show amorphous disks, tidal tails and/or other signs of merger activity; and *late-stage mergers*, if they show a common envelope.

4 Inflow models

4.1 Simulations of merging galaxies

According to simulations of merging massive galaxies, a decrease in the metal content of galaxies, happening shortly after the first pericentre passage³⁸. When star-formation and metal enrichment from supernovae are included³⁷, the dilution is reported to be correlated to the star formation enhancement, and as the merger advances, the dilution is reduced and chemical enrichment becomes dominant. From this last model, the variations in metallicity as well as SFR are considered relatively to the initial conditions on the galaxies (see Figure 4³⁷). In this work, we considered the trends followed by galaxies in interaction with different initial conditions: $Z_{ini}=0.8Z_{\odot}$, $Z_{ini}=0.4Z_{\odot}$ and $Z_{ini}=0.2Z_{\odot}$.

4.2 Inflow model within galaxy evolution

Another model that we consider to reproduce the drop of metallicity in some of the ULIRGs is based on basic equations of chemical evolution. For a standard galaxy, with original stellar mass $M_{*,0}$, SFR ψ , metallicity Z and with α being the fraction in mass of long-lived stars and p the yield of metals (mainly oxygen), we can describe the evolution of gas mass (G), mass of long-lived stars (S) and mass of metals (Z) following the equations⁴²:

$$\dot{G} = -\alpha\psi \quad (1)$$

$$\dot{S} = \alpha\psi \quad (2)$$

$$\dot{Z} = -Z\alpha\psi + p\alpha\psi \quad (3)$$

If a flow A of gas (in either direction) is introduced in the above equations, following the prescriptions⁴², then Equation 1 is modified as:

$$\dot{G} = A - \alpha\psi \quad (4)$$

Thus, we can express Equation 3 in terms of the metal content (Z) as:

$$G\dot{Z} = p\alpha\psi - AZ \quad (5)$$

For our model, we considered that both A and ψ present constant values for most of the evolving time of the galaxy, although to reproduce the massive inflow, we consider that they experience a peak (parameterized as a gaussian distribution), separated by 200 Myr (i.e., the inflow A occurs before the peak in SFR), and we consider that the duration of the infall phase is bigger than the peak of star formation rate (which corresponds to $100 \text{ M}_\odot \text{ yr}^{-1}$). After 1 Gyr of the process, we assume that the effects of outflows are significantly higher, changing the sign of A (from positive to negative). The value of α is computed from the Initial Mass Function⁸², and considering long-lived stars those whose masses range from 0.01_\odot to 3_\odot . Finally, we assume a conservative yield $p=0.003$ ⁸³. As initial conditions, we assume a galaxy with stellar mass 10^{11} M_\odot , mass gas according to the observed ratio⁷⁰, and metallicity $Z=0.84Z_\odot$ according to the obtained plateau in these study for massive galaxies.

Overall, according to this model, the process lasts for 2 Gyr: during which secular evolution is considered only in the first 200 Myr (i.e. both A and ψ show low and constant values). From 300 Myr to 900 Myr, the infall of gas dilutes the metallicity and increases the stellar mass. Finally, after 1 Gyr, the combination of stars polluting the ISM with metals and outflows contribute to enrich the metal content, while stellar mass shows little increase as the peak of star formation has already occurred. The infall process involves a total gas mass of $2.6 \cdot 10^9 \text{ M}_\odot$, which is equivalent to 3% of the stellar mass of the galaxy and 15% of its gas reservoirs.

Methods References

46. Lodders, K. Relative Atomic Solar System Abundances, Mass Fractions, and Atomic Masses of the Elements and Their Isotopes, Composition of the Solar Photosphere, and Compositions of the Major Chondritic Meteorite Groups. *Space Sci. Rev.* **217**, 44 (2021).
47. Houck, J. R. *et al.* The Infrared Spectrograph (IRS) on the Spitzer Space Telescope. *Astrophys. J. Supp.* **154**, 18-24 (2004).
48. Poglitsch, A. *et al.* The Photodetector Array Camera and Spectrometer (PACS) on the Herschel Space Observatory. *Astron. Astrophys.* **518**, L2 (2010).
49. Fernández-Ontiveros, J. A. *et al.* Far-infrared Line Spectra of Active Galaxies from the Herschel/PACS Spectrometer: The Complete Database. *Astrophys. J. Supp.* **226**, 19 (2016).
50. Fischer, C. *et al.* FIFI-LS: The Field-Imaging Far-Infrared Line Spectrometer on SOFIA. *Journal of Astronomical Instrumentation* **7**, 1840003–556 (2018).
51. Imanishi, M. *et al.* AKARI IRC infrared 2-5-5 μm Spectroscopy of a Large Sample of Luminous Infrared Galaxies. *Astrophys. J.* **721**, 1233-1261 (2010).
52. Lebouteiller, V. *et al.* CASSIS: The Cornell Atlas of Spitzer/Infrared Spectrograph Sources. II. High-resolution Observations. *Astrophys. J. Supp.* **218**, 21 (2015).
53. Hernán-Caballero, A. *et al.* The infrared database of extragalactic observables from Spitzer - I. The redshift catalogue. *Mon. Not. R. Astron. Soc.* **455**, 1796-1806 (2016).
54. Spoon, H. W. W. *et al.* The Infrared Database of Extragalactic Observables from Spitzer - II. The Database and Diagnostic Power of Crystalline Silicate Features in Galaxy Spectra. *Astrophys. J. Supp.* **259**, 37 (2022).
55. Inami, H. *et al.* The AKARI 2.5-5 micron spectra of luminous infrared galaxies in the local Universe. *Astron. Astrophys.* **617**, A130 (2018).
56. Sturm, E. *et al.* Mid-Infrared line diagnostics of active galaxies. A spectroscopic AGN survey with ISO-SWS. *Astron. Astrophys.* **393**, 821-841 (2002).
57. Tommasin, S., Spinoglio, L., Malkan, M. A. & Fazio, G. Spitzer-IRS High-Resolution Spectroscopy of 12 μm Seyfert Galaxies. II. Results for the Complete Data Set. *Astrophys. J.* **709**, 1257-1283 (2010).
58. Puget, J. L. & Leger, A. A new component of the interstellar matter: small grains and large aromatic molecules. *ARA&A* **27**, 161-198 (2008).

59. Pérez-Díaz, B., Masegosa, P., Márquez, I. & Pérez-Montero, E. Chemical abundances in the nuclear region of nearby galaxies from the Palomar Survey. *Mon. Not. R. Astron. Soc.* **505**, 4289-4309 (2021).
60. Mollá, M., García-Vargas, M. L. & Bressan, A. PopStar I: evolutionary synthesis model description. *Mon. Not. R. Astron. Soc.* **398**, 451-470 (2009).
61. Pérez-Montero, E. & Amorín, R. Using photo-ionisation models to derive carbon and oxygen gas-phase abundances in the rest UV. *Mon. Not. R. Astron. Soc.* **467**, 1287-1293 (2017).
62. Pérez-Montero, E. *et al.* A bayesian-like approach to derive chemical abundances in type-2 active galactic nuclei based on photoionization models. *Mon. Not. R. Astron. Soc.* **689**, 2652-2668 (2019).
63. Pérez-Montero, E., Amorín, R., Pérez-Díaz, B., Vílchez, J. M. & García-Benito, R. Assessing model-based carbon and oxygen abundance derivation from ultraviolet emission lines in AGNs. *Mon. Not. R. Astron. Soc.* **521**, 1556-1569 (2023).
64. Díaz, A. I. & Zamora, S. On the use of sulphur as a tracer for abundances in galaxies. *Mon. Not. R. Astron. Soc.* **511**, 4377-4392 (2022).
65. Pérez-Montero, E., Díaz, A. I., Vílchez, J. M. & Kehrig, C. An empirical calibration of sulphur abundance in ionised gaseous nebulae. *Astron. Astrophys.* **449**, 193-201 (2006).
66. Kauffmann, G. *et al.* Stellar masses and star formation histories for 10^5 galaxies from the Sloan Digital Sky Survey. *Mon. Not. R. Astron. Soc.* **341**, 33-53 (2003).
67. Brinchmann, J. *et al.* The physical properties of star-forming galaxies in the low-redshift Universe. *Mon. Not. R. Astron. Soc.* **351**, 1151-1179 (2004).
68. Balogh, M. L., Morris, S. L., Yee, H. K. C., Carlberg, R. G. & Ellingson, E. Differential Galaxy Evolution in Cluster and Field. *Astrophys. J.* **527**, 54-79 (1999).
69. Worthey, G. & Ottaviani, D. L. $H\gamma$ and $H\delta$ Absorption Features in Stars and Stellar Populations. *Astrophys. J. Supp.* **111**, 377-386 (1997).
70. Parkash, V., Brown, M. J. I., Jarrett, T. H. & Bonne, N. J. Relationships between HI Gas Mass, Stellar Mass, and Star Formation Rate of HICAT+WISE (HI-WISE) Galaxies. *Astrophys. J.* **864**, A40 (2018).
71. Cluver, M. E., *et al.* Galaxy and Mass Assembly (GAMA): Mid-infrared Properties and Empirical Relations from WISE. *Astrophys. J.* **782**, A90 (2014).
72. Brown, M. J. I. *et al.* Calibration of Ultraviolet, Mid-infrared, and Radio Star Formation Rate Indicators. *Astrophys. J.* **847**, A136 (2017).

73. Cluver, M. E., Jarrett, T. H., Dale, D. A., Smith, J.-D. T., August, T. & Brown, M. J. I. Calibrating Star Formation in WISE Using Total Infrared Luminosity. *Astrophys. J.* **850**, A68 (2017).
74. Sheth, K. *et al.* The Spitzer Survey of Stellar Structure in Galaxies (S4G). *PASP* **122**, 1397 (2010).
75. Muñoz-Mateos, J. C. *et al.* The Impact of Bars on DIsk Breaks as Probed by S⁴G Imaging. *Astrophys. J.* **771**, A49 (2013).
76. Querejeta, M. *et al.* The Spitzer Survey of Stellar Structure in Galaxies (S⁴G): Precise Stellar Mass Distributions from Automated Dust Correction at 3.6 μm . *Astrophys. J. Supp.* **219**, A5 (2015).
77. Muñoz-Mateos, J. C. *et al.* The Spitzer Survey of Stellar Structure in Galaxies (S⁴G): Stellar Masses, Sizes, and Radial Profiles of 2352 Nearby Galaxies. *Astrophys. J. Supp.* **219**, A3 (2015).
78. Bell, E. F., McIntosh, D. H., Katz, Z., Weinberg, M. D. The Optical and Near-Infrared Properties of Galaxies. I. Luminosity and Stellar Mass Functions. *Astrophys. J. Supp.* **149**, 289-312 (2003).
79. Ciesla, L. *et al.* Constraining the properties of AGN host galaxies with spectral energy distribution modelling. *Astron. Astrophys.* **576**, A10 (2015).
80. Boquien, M. *et al.* CIGALE: a python Code Investigating GALaxy Emission. *Astron. Astrophys.* **622**, A103 (2019).
81. Vika, M., Ciesla, L., Charmandaris, V., Xilouris, E. M. & Lebouteiller, V. The physical properties of Spitzer/IRS galaxies derived from their UV to 22 μm spectral energy distribution. *Astron. Astrophys.* **597**, A51 (2017).
82. Kroupa, P. On the variations of the initial mass function. *Mon. Not. R. Astron. Soc.* **322**, 231-246 (2001).
83. Pilyugin, L. S., Thuan, T. X. & Vílchez, J. M. On the maximum value of the cosmic abundance of oxygen and the oxygen yield. *Mon. Not. R. Astron. Soc.* 353-360 (2007).

5 Data Availability Statement

Data supporting this study will be publicly available at the CDS.